Effect of area ratio of the primary nozzle on steam ejector performance considering nonequilibrium condensations

Yang, Yan; Karvounis, Nikolas; Walther, Jens Honore; Ding, Hongbing; Wen, Chuang

Published in:
Energy

Link to article, DOI:
10.1016/j.energy.2021.121483

Publication date:
2021

Document Version
Publisher's PDF, also known as Version of record

Energy 237 (2021) 121483

Contents lists available at ScienceDirect

Energy

journal homepage: www.elsevier.com/locate/energy

Effect of area ratio of the primary nozzle on steam ejector performance considering nonequilibrium condensations

Yan Yang [a], Nikolas Karvounis [b], Jens Honore Walther [b, c], Hongbing Ding [d], Chuang Wen [a, b, *]

[a] Faculty of Engineering, University of Nottingham, Nottingham, NG7 2RD, United Kingdom
[b] Department of Mechanical Engineering, Technical University of Denmark, Nils Koppels Allé, 2800, Kgs. Lyngby, Denmark
[c] Computational Science and Engineering Laboratory, ETH Zürich, Clausiusstrasse 33, CH-8092, Zürich, Switzerland
[d] School of Electrical and Information Engineering, Tianjin University, Tianjin, 300072, China

ARTICLE INFO

Article history:
Received 2 January 2021
Received in revised form
22 April 2021
Accepted 10 July 2021
Available online 13 July 2021

Keywords:
Steam ejector
Nonequilibrium condensation
Supersonic flow
Nanodroplet
Primary nozzle
Area ratio

ABSTRACT

The formation and evaporation of nanodroplets in steam ejectors is neglected in many numerical simulations. We analyse the influence of a primary nozzle on steam ejector performances considering phase change processes. The numerical model is validated in detail against experimental data of supersonic nozzles and steam ejectors available in the literature. The results show that the first nonequilibrium condensation is observed within the primary nozzle, while under-expanded supersonic flow causes a second nucleation-condensation process to achieve a large liquid fraction of 0.26 in the steam ejector. The compression process of the supersonic flow results in a steep decrease of the degree of subcooling leading to droplet evaporations. The condensation and evaporation processes repeat alternatively depending on the flow behaviour in the mixing section. The increasing area ratio leads to the transition of the flow structure from under-expanded flows to over-expanded flows in the mixing section. The droplet diameter is about 7 nm in the constant section and the entrainment ratio can reach approximately 0.75 for an area ratio of 8, which achieves a good performance of the steam ejector.

1. Introduction

A supersonic ejector is a static fluid device designed to achieve high energy efficiency in thermal engineering systems. The main advantage of an ejector is to use the expansion characteristics of high-pressure fluids to entrain low-pressure streams to upgrade low-grade energies [1,2]. Therefore, the supersonic ejector is widely used in many industries, such as refrigeration system [3], seawater desalination [4], renewable energy utilisation [5] and hydrogen energy system [6].

Steam ejectors have attracted extensive attention from theoretical [7], experimental [8] and numerical [9] studies. Computational fluid dynamics (CFD) is powerful to comprehensively evaluate and optimise steam ejectors. The dry gas model can simplify the mathematical model for the prediction of the complex flow behaviour, which is widely used in the numerical evaluation of a steam ejector. Ramesh and Joseph Sekhar [10] ignored the phase change process to evaluate the influence of suction chamber angles on ejector performances utilising the k-ω shear stress transport (SST) model. Wang et al. [11] optimised the primary nozzle profile in steam ejectors using the dry steam assumption and realizable k-ε turbulence model. Ariafar et al. [12] discussed the mixing layer inside steam ejectors ignoring nonequilibrium condensations in supersonic flows employing the k-ω SST model. Tang et al. [13] numerically studied the relationship between the mixing process and entrainment characteristics in steam ejectors based on the dry gas model and realizable k-ε turbulence model. Suvarnakuta et al. [14] employed the dry gas assumption and k-ω SST model to carry out numerical studies on two-stage ejectors. Liu et al. [15] evaluated the effect of an area ratio on entrainment ratios in a steam ejector using the dry gas model and realizable k-ε turbulence model. In these studies, the dry gas assumption was used in steam ejectors by ignoring the phase change process, whose importance has been emphasized in the thermodynamic analysis [16] and experimental observations [17].

The phase change behaviour is complicated in steam ejectors as

* Corresponding author. Faculty of Engineering, University of Nottingham, Nottingham, NG7 2RD, United Kingdom.
E-mail addresses: chuang.wen@nottingham.ac.uk, cwen@mek.dtu.dk (C. Wen).

https://doi.org/10.1016/j.energy.2021.121483

Nomenclature

CFD	computational fluid dynamics
RNG	Re-Normalisation Group
SST	shear stress transport
A	cross-section area of a primary nozzle
d	droplet diameter
E	total energy
h_{fg}	latent heat
I	turbulent intensity
J	nucleation rate
k_B	Boltzmann constant
Kn	Knudsen number
l_0	characteristic dimension
m_v	mass of a vapour molecule
m_p	primary mass flow rate
m_s	secondary mass flow rate
N	droplet number per volume
p	pressure
Pr	Prandtl number
q_c	condensation coefficient
q_{jeff}	effective heat flux
r	droplet radius
r_c	critical droplet radius
Re	Reynolds number
S_{pr}	area ratio of a primary nozzle
Stk	Stokes number
t	time
T	temperature
u	velocity
u'	root-mean-square of turbulent velocity fluctuations
u_{avg}	mean velocity
x	Cartesian coordinates
Y	liquid fraction
β	modelling parameter
Γ	mass generation rate due to condensation process
ΔT	subcooling
λ_v	vapour conductivity
ν	modelling correction coefficient
ξ	entrainment ratio
ρ	density
μ_g	gas dynamic viscosity
σ	surface tension
τ_{ij}	viscous stress
φ	temperature correction coefficient

Subscript

c	critical condition
i, j	Cartesian tensor notation
l	liquid phase
out	outlet of a primary nozzle
p	droplet
pr	primary nozzle
s	saturation condition
th	throat of a primary nozzle
v	vapour phase

the formation and evaporation of the massive nanodroplets intensely interact with the violent turbulent flow, mixing process, flow separation and shock waves. Ariafar et al. [18] and Wang et al. [19] carried out numerical simulations on the steam condensation in a primary nozzle (not a whole steam ejector) using realizable k-ε and Re-Normalisation Group (RNG) k-ε models, respectively. Marynowski et al. [20] employed the standard k-ε model to compute the phase changes within a steam ejector using the build-in nonequilibrium condensation model in the commercial software ANSYS Fluent. Sharifi et al. [21], Zhang et al. [22] and Wen et al. [23] employed realizable k-ε, RNG k-ε and k-ω SST turbulence models, respectively, to compare the dry gas and condensing flow models in evaluating ejector performances. The impact of the back pressure on fluid flows inside a steam ejector was numerically studied using a condensing flow model and k-ω SST model [24]. Zhang et al. [25] optimised the primary nozzle profile considering nonequilibrium condensations with the k-ω SST turbulence model. Faghih Aliabadi and Bahiraei [26] numerically investigated the influence of an injection of water nanodroplets from the primary nozzle inlet on ejector performances and found that an injection of 0.4% wetness nanodroplet could decrease 2.6% entrainment ratios. These studies demonstrated the significance of the phase change behaviour for ejector performance evaluations.

Regarding the optimisation of the primary nozzle in steam ejectors, most numerical studies were carried out based on the dry steam assumption. Yang et al. [27] employed the dry steam model to investigate the effect of the primary nozzle structure on the steam ejector performance using five shapes of conical, elliptical, square, rectangular and cross-shaped nozzles. Sharifi & Sharifi [28] numerically studied the impact of the primary nozzle, namely, the lengths of the converging and diverging parts, outlet diameter, on the steam ejector performance based on the dry steam model. Similarly, Fu et al. [29] and Wu et al. [30] assumed the dry steam model to predict the influence of the outlet diameter of the primary nozzle on the performance of steam ejectors. Wang et al. [19] investigated the effect of the outlet diameter of the nozzle on the condensation parameters in a supersonic nozzle, which can hardly be extended to a steam ejector as the flow behaviour in the mixing section and the entrainment performance are not discussed in their numerical simulations. Hence, the geometrical optimisation of the primary nozzle needs to be further investigated considering the phase change to better understand the flow behaviour and entrainment performance for the design and application of steam ejectors.

It can be summarised that the challenge of the numerical simulation in steam ejectors is to interact the nonequilibrium condensation with the turbulent flow, mixing process, and shock waves. On the one hand, many numerical simulations assumed the dry gas model to simplify the numerical modelling by ignoring the phase change in steam ejectors. On the other hand, various turbulence models are used for flow behaviour predictions in steam ejectors, such as k-ε family (standard, realizable and RNG) and k-ω SST. A validation of turbulence models is required to establish an accurate prediction of the complex flow structure considering the phase change process in steam ejectors.

In the present study, a nonequilibrium condensing flow model is first developed to assess the turbulence modelling for the numerical simulation of steam ejectors. Then, the complicated flow behaviour, including the supersonic flow, nonequilibrium condensation, mixing process and shock waves, are validated in detail against experimental data from both nozzle and ejector cases. The effect of the area ratio of the primary nozzle on the flow behaviour and entrainment ratios are further investigated using the wet steam model to describe the heat and mass transfer in the phase change process. The transition of the flow structures from under-expanded flows to over-expanded flows is reported due to the

increase of the area ratio of the primary nozzle in the steam ejector.

2. Steam ejector

Fig. 1 illustrates the principle of a steam ejector, which includes a primary nozzle, a suction chamber, mixing and constant sections, and a diffuser [31,32]. The two-dimensional (2D) axisymmetry [33] and three-dimensional (3D) [34] geometries were employed to model steam ejectors. Pianthong et al. [35] carried out 2D-axisymmetry and 3D simulations for steam ejectors, and showed that the 2D and 3D models predicted similar static pressures at the central line. Sharifi [36] performed a detailed comparison between 2D and 3D simulations for steam ejectors. It was found that similar flow parameters were obtained along the ejector central line including the steam velocity, static pressure, static temperature and Mach number. Meanwhile, both the 2D and 3D numerical entrainment ratios agreed well with experimental data. Therefore, the 2D-axisymmetry model of steam ejectors is employed in this study. The primary nozzle throat diameter is 4.00 mm and the diameter of the constant section of steam ejectors is 14.60 mm. The detailed dimension is shown in Table 1. The quadrilateral mesh is generated for the numerical simulation, as shown in Fig. 2.

3. Mathematical model

Navier-Stokes equations are used to govern the steam ejector flows. The Stokes number, Stk, is a dimensionless number characterising the behaviour of droplets suspended in fluid flows:

$$\mathrm{Stk} = \frac{\rho_p {d_p}^2 u}{18 \mu l_0} \tag{1}$$

where ρ_p and d_p are the droplet density and diameter, μ is the dynamic viscosity, u is the fluid velocity and l_0 is the characteristic dimension.

The droplet diameter of water in the supersonic condensation is very small, i.e., usually less than 0.1 μm under low-pressure conditions [37,38], thus we use 0.1 μm to evaluate the Stokes number here. It is assumed that the maximum velocity of the steam is 1420 m/s, the water density is 1000 kg m^{-3}, the steam dynamic viscosity is 0.01 × 10^{-3} Pa s, and the characteristic dimension is the diameter of the constant section of steam ejectors, 14.60 mm. The Stokes number is subsequently 0.0054, which illustrates that the droplets follow fluid streamlines very closely. Thus, the no-slip phase velocities are used in this numerical simulation. The liquid fraction and droplet number equations are governing phase change processes within steam ejectors [39,40]:

Continuity equation:

$$\frac{\partial \rho}{\partial t} + \frac{\partial (\rho u_j)}{\partial x_j} = -\Gamma \tag{2}$$

Momentum equation:

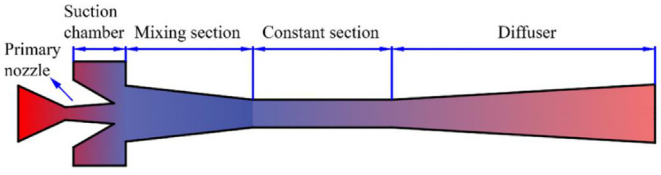

Fig. 1. Steam ejector schematic.

Table 1
Dimension of the steam ejector.

Steam ejector dimension	Size (mm)
Inlet diameter of the primary nozzle	10.00
Throat diameter of the primary nozzle	4.00
Outlet diameter of the primary nozzle	7.00
Length of the converging part of the primary nozzle	17.00
Length of the diverging part of the primary nozzle	28.62
Inlet diameter of the mixing chamber	16.00
Length of the mixing chamber	45.79
Diameter of the constant section	14.60
Length of the constant section	54.00
Outlet diameter of the diffuser	24.00
Length of the diffuser	134.59

$$\frac{\partial}{\partial t}(\rho u_i) + \frac{\partial}{\partial x_j}(\rho u_j u_i) = -\frac{\partial p}{\partial x_i} + \frac{\partial \tau_{ij}}{\partial x_j} - u_i \Gamma \tag{3}$$

Energy equation:

$$\frac{\partial (\rho E)}{\partial t} + \frac{\partial}{\partial x_i}[u_i(\rho E + p)] = \frac{\partial q_{jeff}}{\partial x_j} + \frac{\partial}{\partial x_j}(u_i \tau_{ij}) - h_{fg}\Gamma \tag{4}$$

Liquid fraction transport equation:

$$\frac{\partial (\rho Y)}{\partial t} + \frac{\partial}{\partial x_j}(\rho Y u_j) = \Gamma \tag{5}$$

Droplet number transport equation:

$$\frac{\partial (\rho N)}{\partial t} + \frac{\partial}{\partial x_j}(\rho N u_j) = \rho J \tag{6}$$

where Γ presents the mass generation rate due to the condensation process [41]:

$$\Gamma = \frac{4\pi {r_c}^3}{3}\rho_l J + 4\pi r^2 \rho_l N \frac{dr}{dt} \tag{7}$$

The nucleation rate, J, adopts modified classical nucleation theory [42]:

$$J = \frac{q_c}{1+\varphi}\frac{{\rho_v}^2}{\rho_l}\sqrt{\frac{2\sigma}{\pi {m_v}^3}}\exp\left(-\frac{4\pi\sigma}{3k_B T_v}{r_c}^2\right) \tag{8}$$

The droplet growth rates are predicted by Young's model [43]:

$$\frac{dr}{dt} = \frac{\lambda_v (T_s - T_v)}{\rho_l h_{fg} r} \frac{(1 - r_c/r)}{\left(\frac{1}{1+2\beta \mathrm{Kn}} + 3.78(1-\nu)\frac{\mathrm{Kn}}{\mathrm{Pr}}\right)} \tag{9}$$

$$\Delta T = T_s - T_v \tag{10}$$

where ΔT is the degree of subcooling, and other definitions of the variables can be found in the nomenclature ($q_c = 1.0$, $\beta = 0.0$ in this study [44]).

The computations are carried out by ANSYS Fluent 18 [45]. The liquid fraction and droplet number equations are added into Fluent using C programming [46]. The inlet boundaries at nozzle and suction entrances are assumed to the pressure inlet, and pressure outlet boundaries are set to the ejector outlet. The quadrilateral meshes are used for all the nozzles and steam ejectors in this study based on the grid independent tests. The k-ω SST model is considered for the turbulent flow within steam ejectors, and the turbulent intensity is presented as follows [47]:

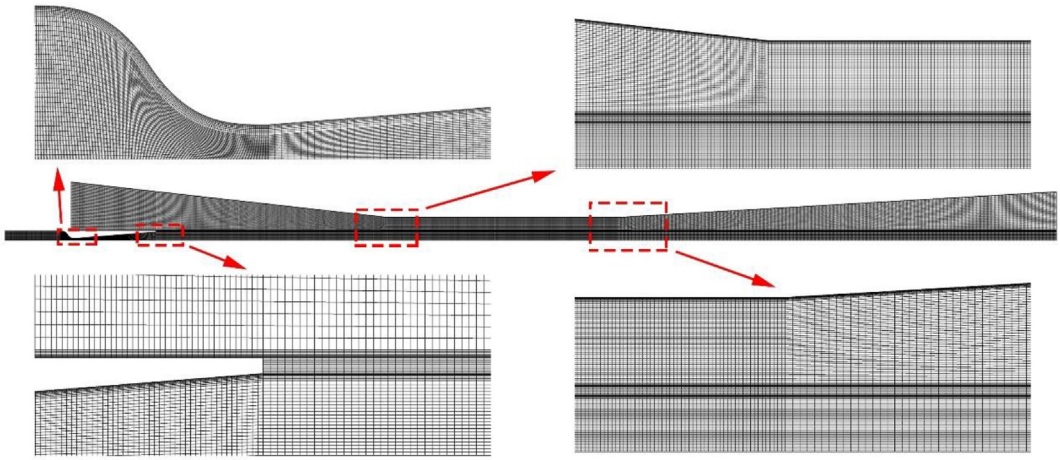

Fig. 2. Computational grid for the steam ejector.

$$I = \frac{u'}{u_{avg}} = 0.16\mathrm{Re}^{-1/8} \tag{11}$$

where Re is the Reynolds number, I is the turbulent intensity.

4. Results and discussion

4.1. Roles of turbulence models in predicting steam ejector performances

4.1.1. Nonequilibrium condensation in supersonic flows without shock waves

The numerical validations are performed for evaluating the influence of turbulence models on supersonic condensations without shock waves. The supersonic nozzle and operating conditions are obtained from the experimental test conducted by Gyarmathy [48]. The operating parameters include the total pressure of 89 bar and total temperature of 619.96 K at the nozzle inlet. The back pressure is assumed at 100 Pa to achieve a supersonic flow condition. Fig. 3 shows the wall pressure and droplet numbers in the supersonic flow based on k-ε Standard, RNG, Realizable and k-ω SST models, as well as a case of laminar flow. It can be found that all of the turbulence models from k-ε families to k-ω SST predict similar pressure and droplet radius. The numerical calculations agree well with experimental data. This indicates that the turbulence models from k-ε family to k-ω SST show very similar performance in predicting steam condensations in supersonic flows without shock waves.

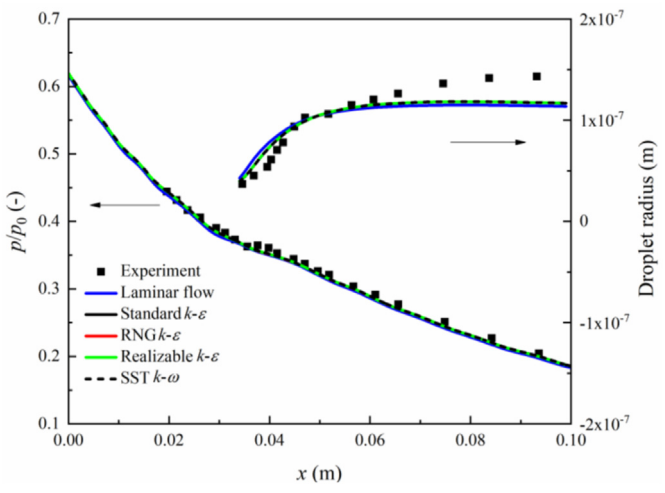

Fig. 3. Effect of turbulence model on the nonequilibrium condensation within the supersonic flow without shock waves [48].

4.1.2. Nonequilibrium condensation in supersonic flows with shock waves

The shock wave is a key flow structure inside a supersonic ejector, which is expected to be affected by the turbulence modelling. Thus, we employ the experimental test presented by Binnie and Green in a Laval nozzle [49] to assess the influence of turbulence modelling on condensations and shock waves in supersonic flows. Fig. 4 illustrates the static pressure profile along with the Laval nozzle showing the occurrence of shock waves in supersonic flows. By comparing the numerical and experimental results, all four models capture almost the same onset of steam condensations. However, the position of the shock wave differs significantly from the four turbulence models. The shock waves

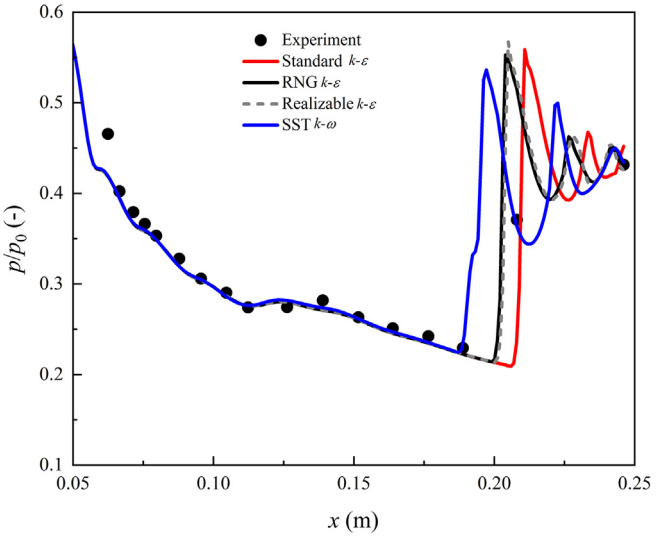

Fig. 4. Pressure profiles at the central line in the Binnie and Green's Laval nozzle [49]. (For interpretation of the references to colour in this figure legend, the reader is referred to the Web version of this article.)

appear within nozzle diverging parts at around $x = 0.19$ m for k-ω SST model. The k-ε turbulence models predict shock wave positions further downstream at around $x = 0.21$ m for the standard k-ε model, and $x = 0.20$ m for RNG and realizable k-ε models. For this case, standard k-ε and k-ω SST models capture the Wilson point and shock position against experimental data.

4.1.3. Shock waves in supersonic flows without nonequilibrium condensations

Based on the aforementioned validation and discussion of the four turbulence models for nonequilibrium condensations in supersonic flows, Hunter's experiments [50] are employed to further investigate the capability of standard k-ε and k-ω SST models in shock predictions in supersonic flows without condensation behaviours. The comparisons between the computed and experimental pressure profiles along with the convergent-divergent nozzle are depicted in Fig. 5 (a). The k-ω SST model agrees well with the experimental measurements to predict the onset of shock waves, while the standard k-ε modelling computes later shock positions. Hence, the standard k-ε modelling is slow to respond to the flow separation in supersonic flows, as shown in Fig. 5 (b)–(c).

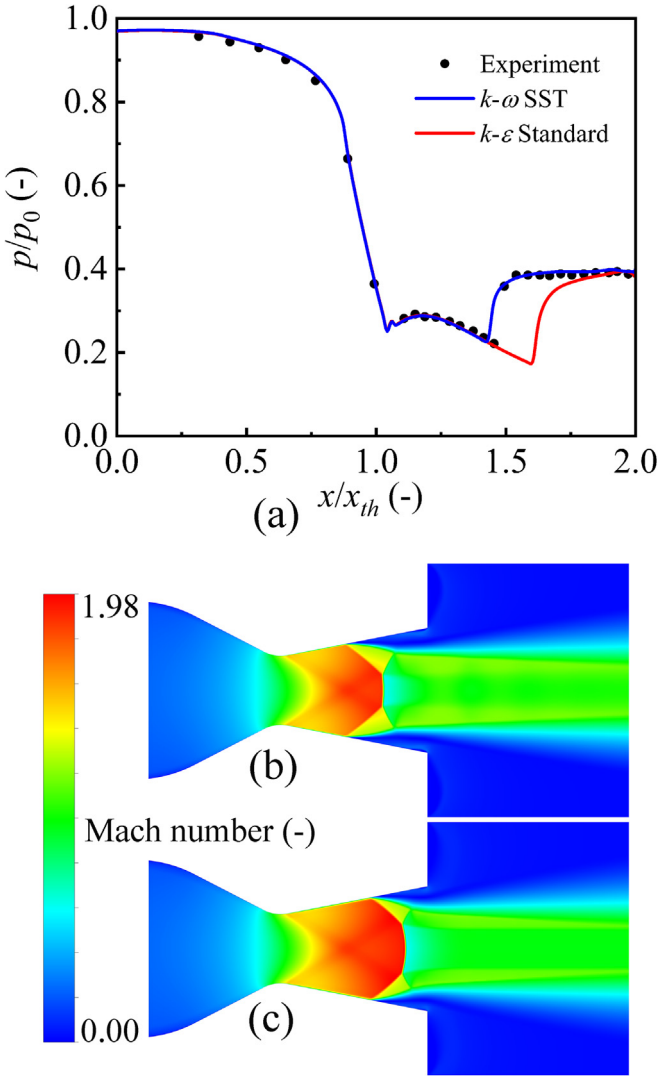

Fig. 5. The Hunter's nozzle [50] results: pressure comparison between the simulations and experiments (a), Mach number contours using k-ω SST model (b) and k-ε standard model (c).

For this case, the k-ω SST turbulence model represents a good prediction of the shock structure in a supersonic flow.

In general, based on the validation of the numerical results with experimental data from Gyarmathy's [48], Binnie and Green's [49] and Hunter's nozzles [50], the k-ω SST turbulence model shows a good performance in predicting nonequilibrium condensations and shock waves in the supersonic flow.

4.1.4. Model validation for the steam ejector

Following the aforementioned solid validations of the turbulence model, the k-ω SST modelling and wet steam model are used to investigate ejector performances. The entrainment ratio, ξ, is defined as the ratio of the mass flow rate of the secondary flow, m_s, to the mass flow rate of the primary flow, m_p.

$$\xi = \frac{m_s}{m_p} \tag{12}$$

The entrainment ratio determines the mass flow that can be entrained from the suction chamber. Fig. 6 illustrates the comparison between experimental [51] and numerical results [33]. The numerical pressure agrees well with experimental data. The numerical model also gives an entrainment ratio of 0.294 compared to the experimental value of 0.31 within the steam ejector, which demonstrates that the simulation agrees well with experimental data. This indicates that the wet steam model considering nonequilibrium condensation processes can accurately evaluate the performance of steam ejectors.

4.2. Nonequilibrium condensations in steam ejectors

The structure and dimensions of the steam ejector used in the numerical simulation are described in Fig. 1 and Table 1 in Section 2. The flow structures within steam ejectors are described in Figs. 7–11. The Mach numbers in Fig. 7 demonstrate that the steam expands to supersonic flows within the diverging part of the primary nozzle. The under-expanded supersonic flows are achieved in the mixing section with a maximum Mach number of 3.99 in this case, which induces the low pressure to entrain secondary steams from the suction entrance. The motive and secondary steams mix in the mixing and constant sections, and finally discharge from the outlet of the ejector.

During the expansion within the primary nozzle, the steam reaches a nonequilibrium state inside the diverging part, where the degree of subcooling can reach 32 K as shown in Fig. 8. This generates the first nonequilibrium condensation process and the maximum nucleation rate is 4×10^{24} m^{-3} s^{-1} as shown in Fig. 9. The under-expanded supersonic flow causes a further nonequilibrium state, where the second nonequilibrium condensation occurs in the mixing section. However, the degree of subcooling declines steeply to −60 K due to the compression process of the supersonic flow. The evaporation occurs in this compression process. The condensation and evaporation processes will repeat alternatively inside the mixing section depending on the expansion and compression of the supersonic flow. The condensed droplet diameter can reach approximately 20 nm in the primary nozzle. The size of the condensed nanodroplets varies due to the evaporation-condensation processes in the mixing section, which stay at around 8 nm in the constant section as seen in Fig. 10. Fig. 11 illustrates that the liquid fractions appear inside the nozzle diverging portion. The under-expanded flow induces an increased liquid phase with the maximum value of 0.26 at the first expansion process in the mixing section. The following compression process of the supersonic flow induces a sharp decrease of the liquid fraction to 0.16, which also demonstrates the occurrence of the evaporation

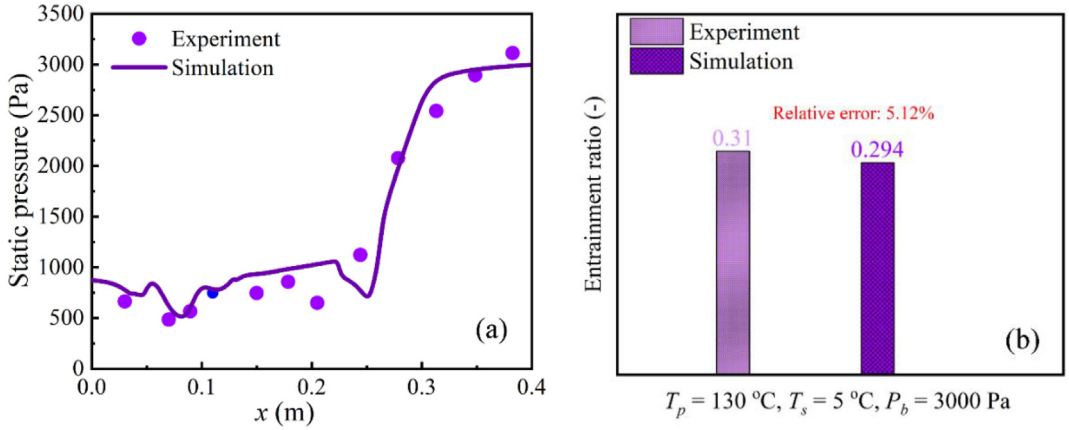

Fig. 6. Wall pressure and entrainment ratio within the steam ejector [51].

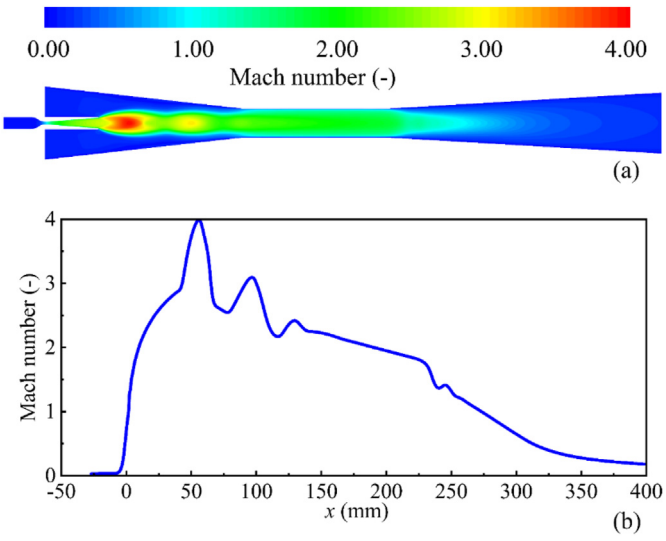

Fig. 7. Mach numbers within a steam ejector.

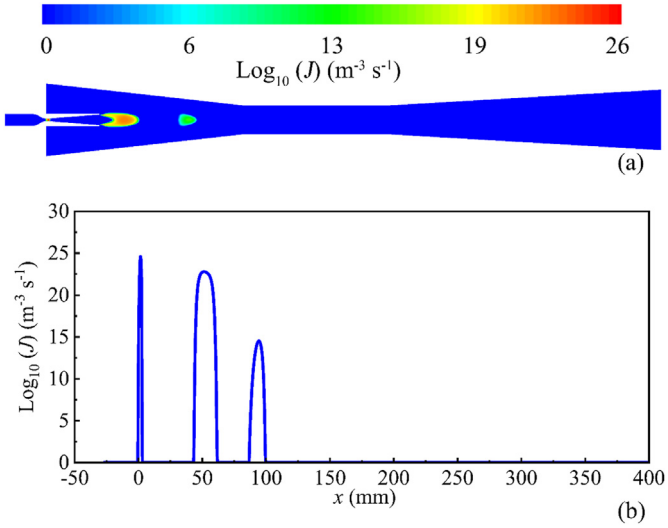

Fig. 9. Nucleation rate within a steam ejector.

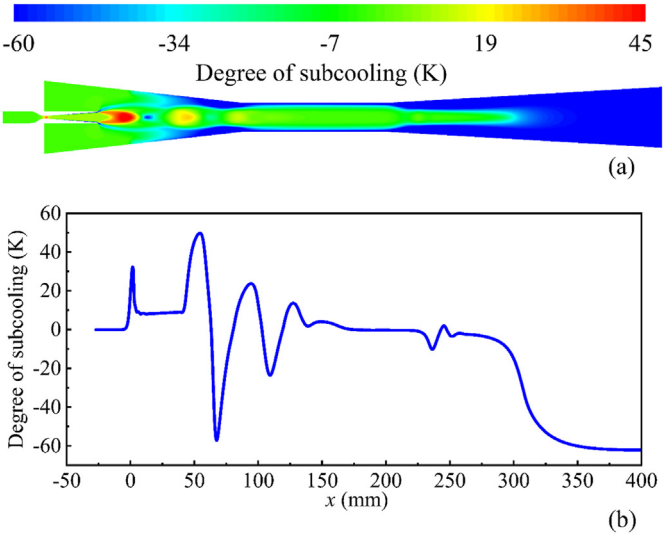

Fig. 8. Degree of subcooling within a steam ejector.

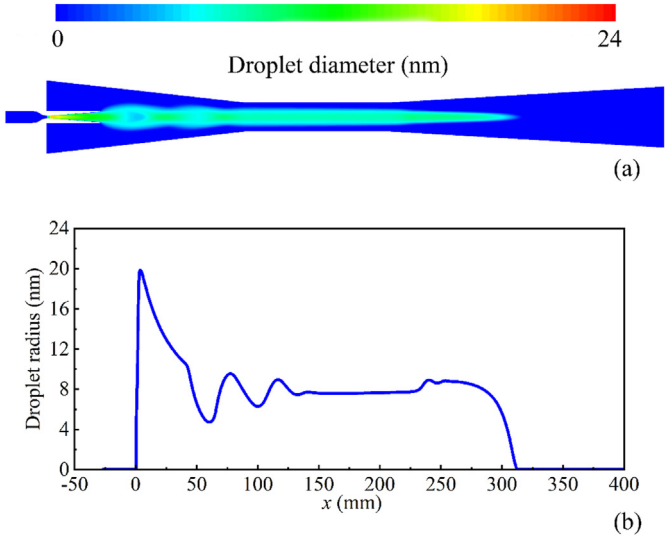

Fig. 10. Droplet diameter within a steam ejector.

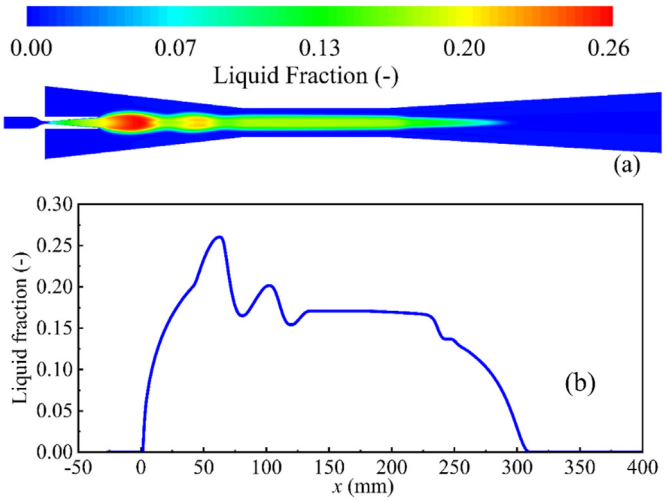

Fig. 11. Liquid fraction within a steam ejector.

process of the condensed droplets. After multiple condensation-evaporation processes, the liquid fraction finally remains at approximately 0.17 inside the constant section. This illustrates that the flow structure within steam ejectors is a gas-liquid two-phase flow within the nozzle diverging part, mixing and constant sections, and diffusers.

4.3. Effect of the primary nozzle on steam ejector performances

The primary nozzle plays a significant role in a steam ejector, in which the steam expands to the supersonic flow in the divergent portion. Meanwhile, the exit of the primary nozzle is connected to the mixing section of the steam ejector, where the high-pressure primary fluid strongly interacts with the low-pressure secondary fluid from the suction chamber, which will not only determine the entrainment performance but also influence the flow structure in steam ejectors. The effect of the area ratio of the primary nozzle on the flow structure and entrainment performance of the steam ejector is investigated considering the phase change process. The

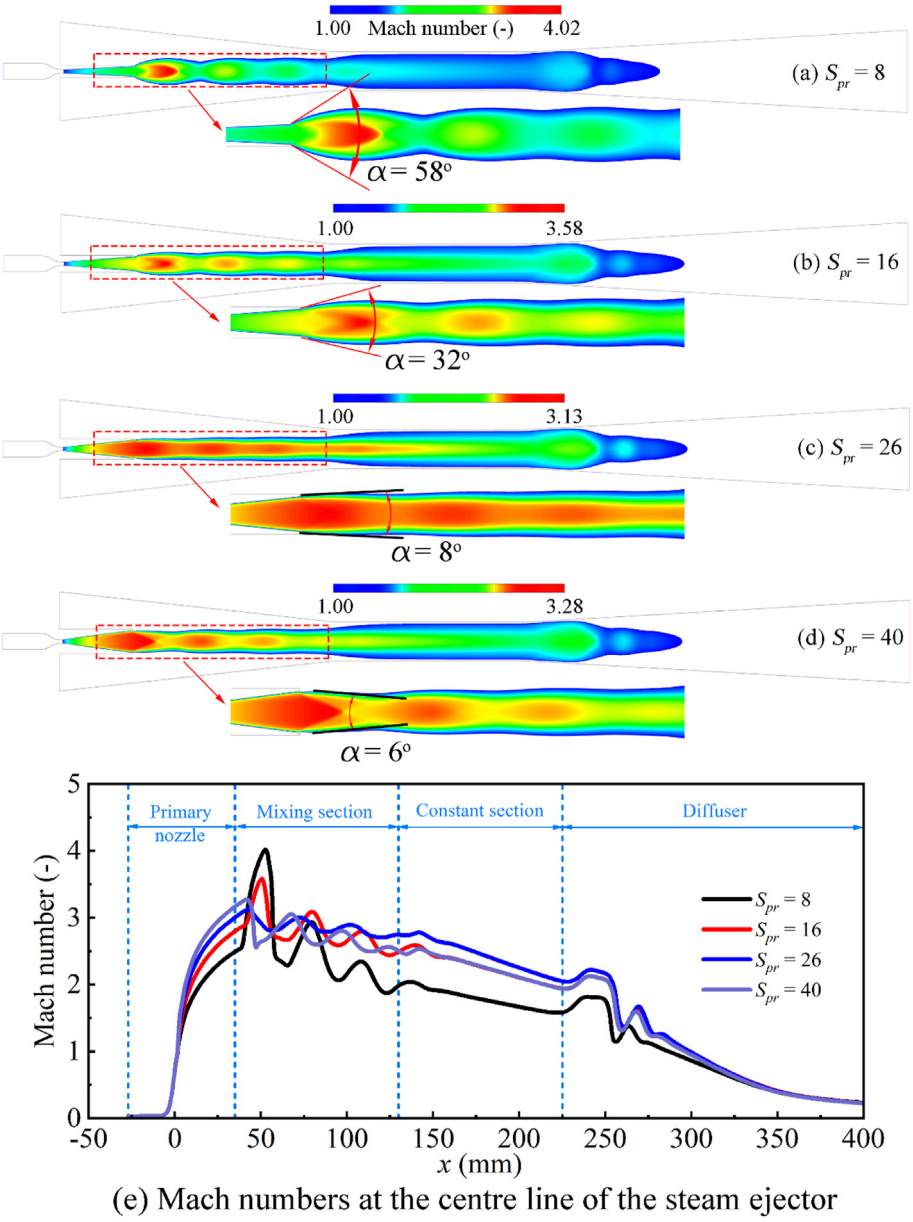

Fig. 12. Mach numbers in steam ejectors with different area ratios (S_{pr}) of the primary nozzle.

Table 2
Computational boundary conditions of a steam ejector.

Boundary conditions	Inlet of a primary nozzle	Inlet of the suction chamber	Outlet of the steam ejector
Total pressure	270,000 Pa	1600 Pa	3000 Pa
Total temperature	403.15 K	287.20 K	297.25 K

area ratio, S_{pr}, is defined as:

$$S_{pr} = \frac{A_{out}}{A_{th}} \tag{13}$$

where A_{out} and A_{th} are the area of the exit cross-section and throat cross-section of the primary nozzle, respectively.

The different primary nozzles with an area ratio of $S_{pr} = 8$, 16, 26 and 40 are employed to conduct the comparison studies, while the other parts of the steam ejector remain unchanged. The Mach number and static pressure at $S_{pr} = 8$, 16, 26 and 40 are described in Figs. 12–13. Table 2 gives the details about the computational boundary conditions. The higher area ratio results in stronger expansions and higher Mach numbers in primary nozzles. For instance, the Mach number at the nozzle outlet can reach 2.49, 2.80, 3.00 and 3.16 for $S_{pr} = 8$, 16, 26 and 40, respectively. The increasing area ratio of the primary nozzle from 8 to 40 leads to the transition of the flow structure from under-expanded flows to over-expanded flows in the mixing section. This can be further illustrated by the pressure contours in the nozzle divergent part and mixing section in Fig. 13. For the area ratio of $S_{pr} = 8$, the static pressure at the nozzle exit of about 6657 Pa is higher than surrounding pressures. The steam expands in the mixing section and the maximum Mach number can reach approximately 4, where the divergence angle of the under-expanded flow is about 58°. When the area ratio increases to $S_{pr} = 16$, the static pressure at the nozzle outlet is 3012 Pa, which still induces a moderate under-expanded flow with a divergence angle of 32°. For the area ratio of $S_{pr} = 26$, the high expansion capacity of the primary nozzle achieves a static pressure of 1615 Pa at the nozzle exit which is very close to the surrounding pressure of 1582 Pa. The steam subsequently presents a slight expansion in the mixing section and the peak value of the Mach number is only around 3 with a divergence angle of 8° under this condition. The static pressure is about 1011 Pa at the nozzle exit, which is much lower than surrounding pressures at $S_{pr} = 40$. The steam is compressed when it reaches the mixing section, which presents an over-expanded flow with a convergence angle of 6°. This indicates that the increasing area ratio from $S_{pr} = 26$ to $S_{pr} = 40$ results in the transition of the flow structure from under-expanded flows to over-expanded flows in the mixing section. This flow structure transition also slightly decreases the Mach number in mixing and constant sections.

The different flow structures due to the various area ratio of the primary nozzle further affect the formation and evaporation processes of the nanodroplets inside steam ejectors. The condensation parameters in the steam ejector under the four different area ratios of the primary nozzle are illustrated in Fig. 14. The homogenous nucleation process is achieved in the primary nozzle for all cases, although there are slight differences among the nucleating region as shown in Fig. 14 (a). However, the different flow structures in the mixing section induce various nucleation behaviours of the steam. The stronger under-expanded flow for the area ratio of $S_{pr} = 8$ induces another two homogeneous nucleation processes in the mixing section. The moderate under-expanded flow for the area ratio of $S_{pr} = 16$ generates another one nucleation process in the mixing section, while nonequilibrium condensations do not appear inside the mixing section at $S_{pr} = 26$ and $S_{pr} = 40$. Fig. 14 (b) shows

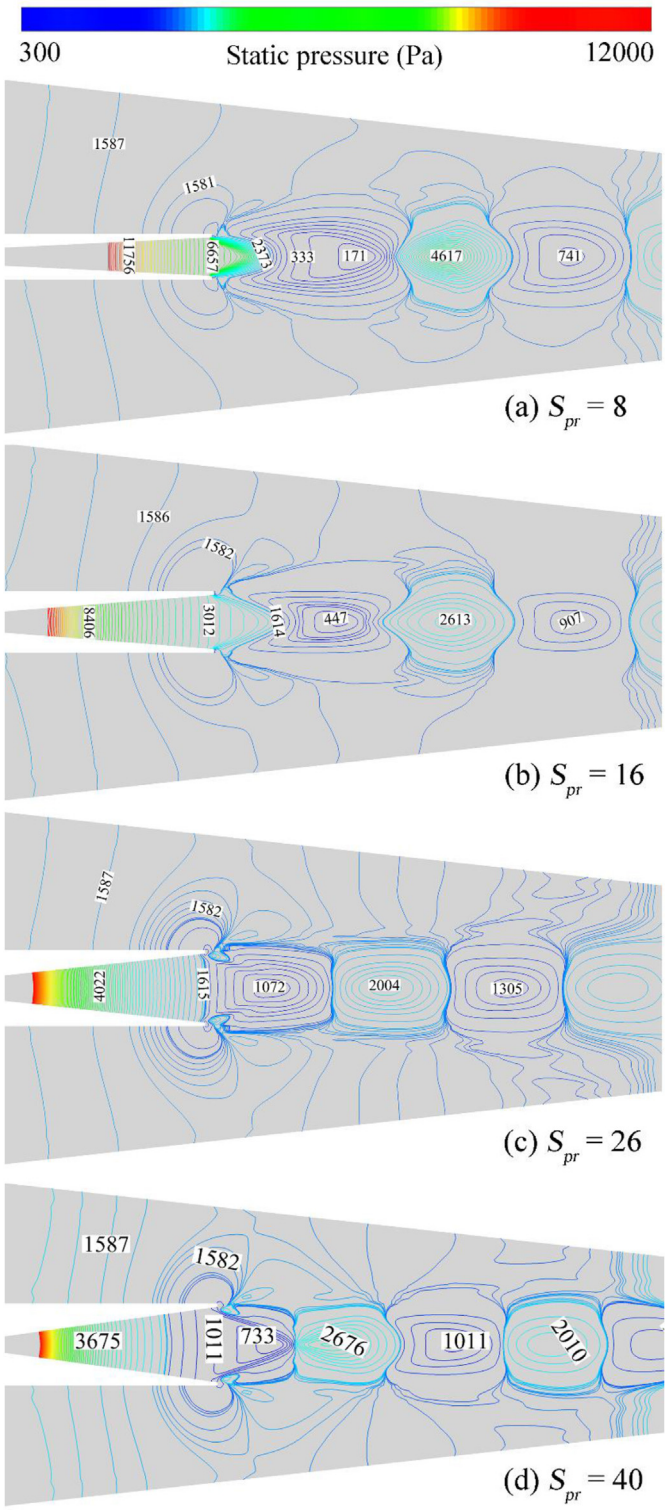

Fig. 13. Static pressure (Pa) in steam ejectors with different area ratios (S_{pr}) of the primary nozzle.

that the nanodroplets are generated due to the nonequilibrium condensation in the steam ejector. For instance, the area ratio of $S_{pr} = 8$ produces a maximum diameter of the condensed droplet of approximately 22 nm in the primary nozzle. The stronger under-expanded flow in the mixing section for the area ratio of $S_{pr} = 8$ results in a more remarkable decrease of the diameters of the condensed droplet compared to the other three cases. The droplet diameters are around 7 nm inside the constant section for the area ratio of $S_{pr} = 8$ compared to the 10 nm droplets for the area ratio of $S_{pr} = 26$. Subsequently, the liquid fraction in the constant section increases from 0.13 for the area ratio of $S_{pr} = 8$ to more than 0.20 for the other three cases. It also can be seen that the transition of the flow structures from under-expanded flows at $S_{pr} = 26$ to over-expanded flows at $S_{pr} = 40$ reduces the droplet size and liquid fraction in mixing and constant sections in the steam ejector.

Fig. 15 illustrates the impact of the area ratio of the primary nozzle on the entrainment ratio and averaged liquid fraction. The entrainment ratio decreases from 0.75 for $S_{pr} = 8$ to 0.70 for $S_{pr} = 26$ with a reduction of about 6.7%. The averaged liquid fraction increases from 0.0069 for $S_{pr} = 8$ to 0.010 for $S_{pr} = 26$, which represents an increase of approximately 45%. The averaged liquid fraction slightly decreases to 0.097 for $S_{pr} = 40$. This indicates that a larger area ratio of the primary nozzle not only reduces the entrainment capacity from the suction chamber but also leads to more liquid fractions in the steam ejector.

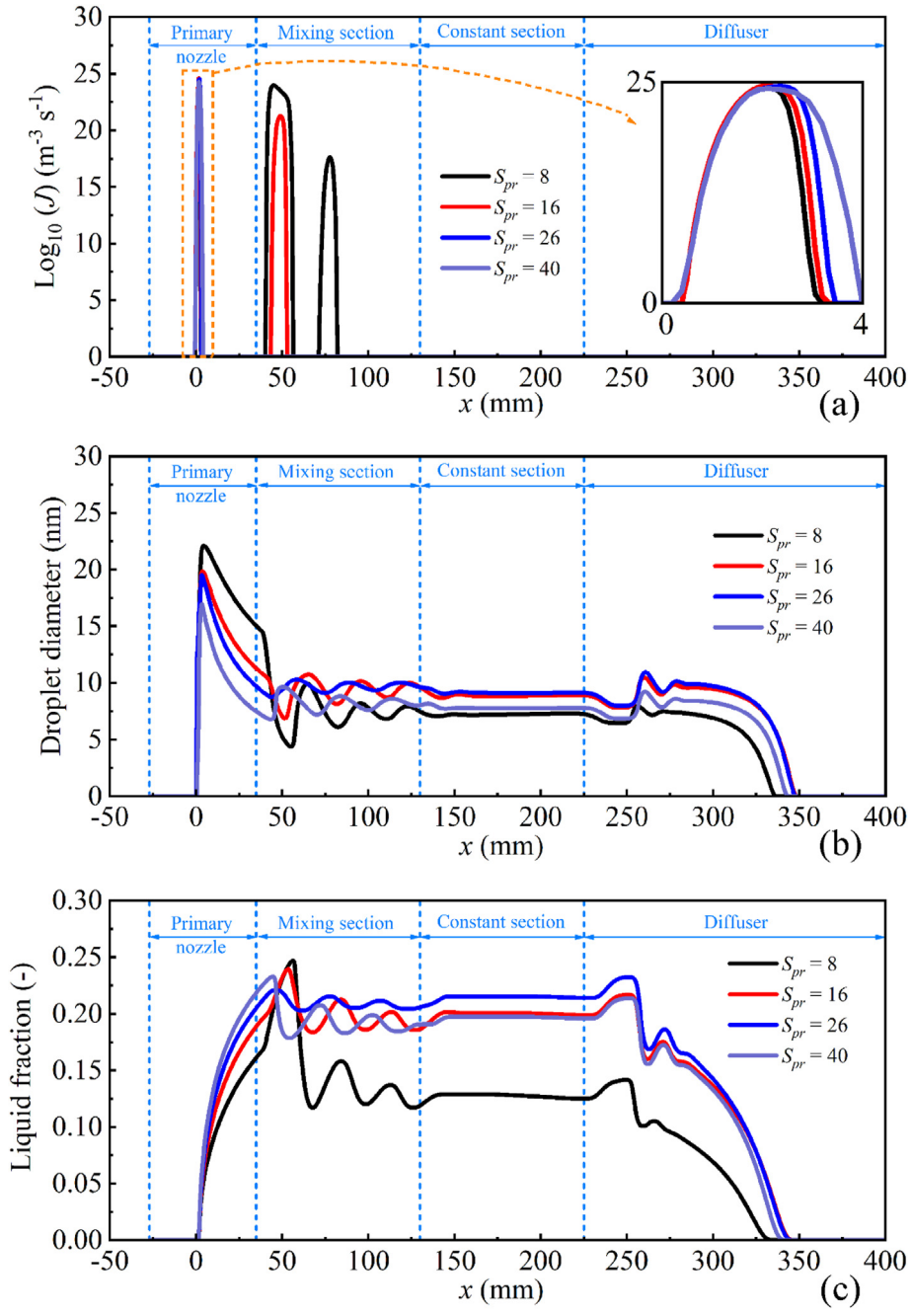

Fig. 14. Condensation parameters in steam ejectors with different area ratios (S_{pr}) of the primary nozzle: nucleation rate (a), droplet diameters (b) and liquid fraction (c).

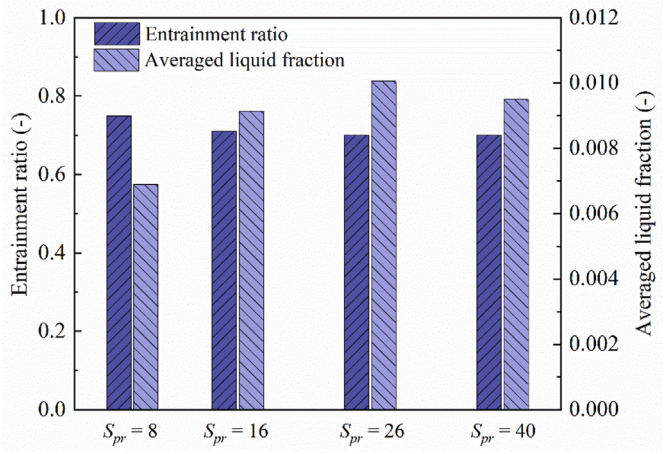

Fig. 15. Entrainment ratio and averaged liquid fraction steam ejectors with different area ratios (S_{pr}) of the primary nozzle.

4.4. Effect of dry and wet steam models on steam ejector performances at different area ratios of the primary nozzle

The impact of the wet steam and dry steam models on steam ejector performances is evaluated at different area ratios of the primary nozzle. In the dry steam model, the phase change of the steam is neglected and subsequently, the heat and mass transfer is not considered in numerical modellings. The flow parameters are compared at different area ratios of the primary nozzle $S_{pr} = 8$ and $S_{pr} = 40$, as shown in Figs. 16–18. It can be seen that the dry steam model predicts lower pressure and temperature than wet steam simulation in the primary nozzle, which means that the dry steam model over-predicts the steam expansion in the ejector. From the static temperature distributions in Fig. 17, we can see that there is a steep temperature jump in the primary nozzle in wet steam simulations. This is because that the latent heat released from the phase change process heats the vapour phase, which demonstrates the significance of supersonic condensations in modelling the flow behaviour in steam ejectors.

The difference between dry and wet steam models can be further illustrated in the contours and profiles of Mach numbers in Fig. 18. For $S_{pr} = 8$, the wet steam model calculates a maximum Mach number of 4.02, which is exaggeratedly up to 6.12 in the dry steam model. Similar results are observed for $S_{pr} = 40$ that the wet and dry steam models calculate the peak value of the Mach number of 3.27 and 5.05, respectively. This also demonstrates that the dry steam assumption over-predicts the steam expansion in steam ejectors due to the neglect of the heat and mass transfer in the phase change process. The dry and wet steam models also show differences in flow structures in the mixing section and diffuser. For instance, the dry steam model predicts an earlier position of the

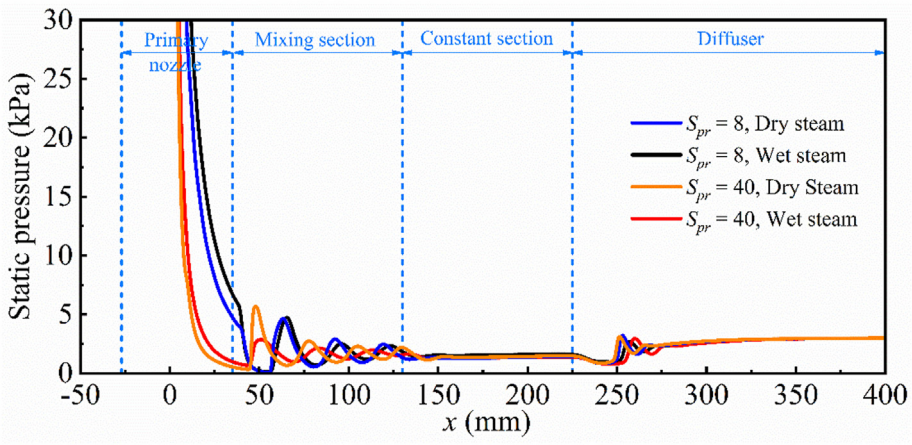

Fig. 16. Effect of wet steam and dry steam models on the static pressure in the steam ejector at the area ratios of the primary nozzle, $S_{pr} = 8$ and $S_{pr} = 40$.

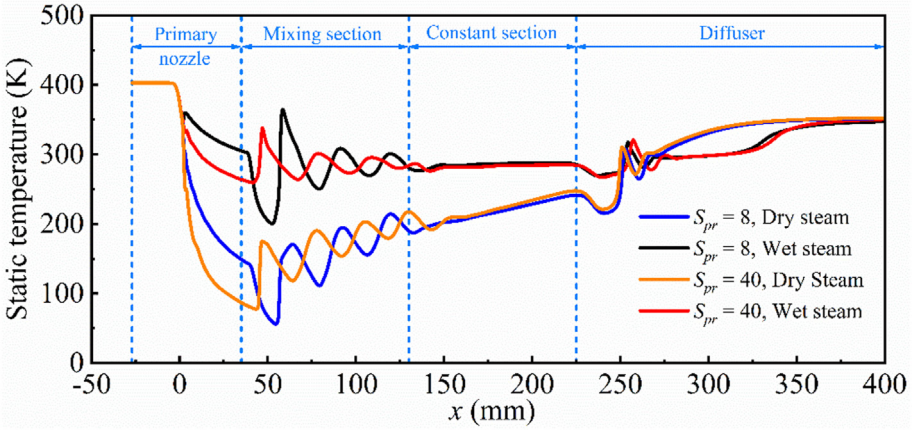

Fig. 17. Effect of wet steam and dry steam models on the static temperature in the steam ejector at the area ratios of the primary nozzle, $S_{pr} = 8$ and $S_{pr} = 40$.

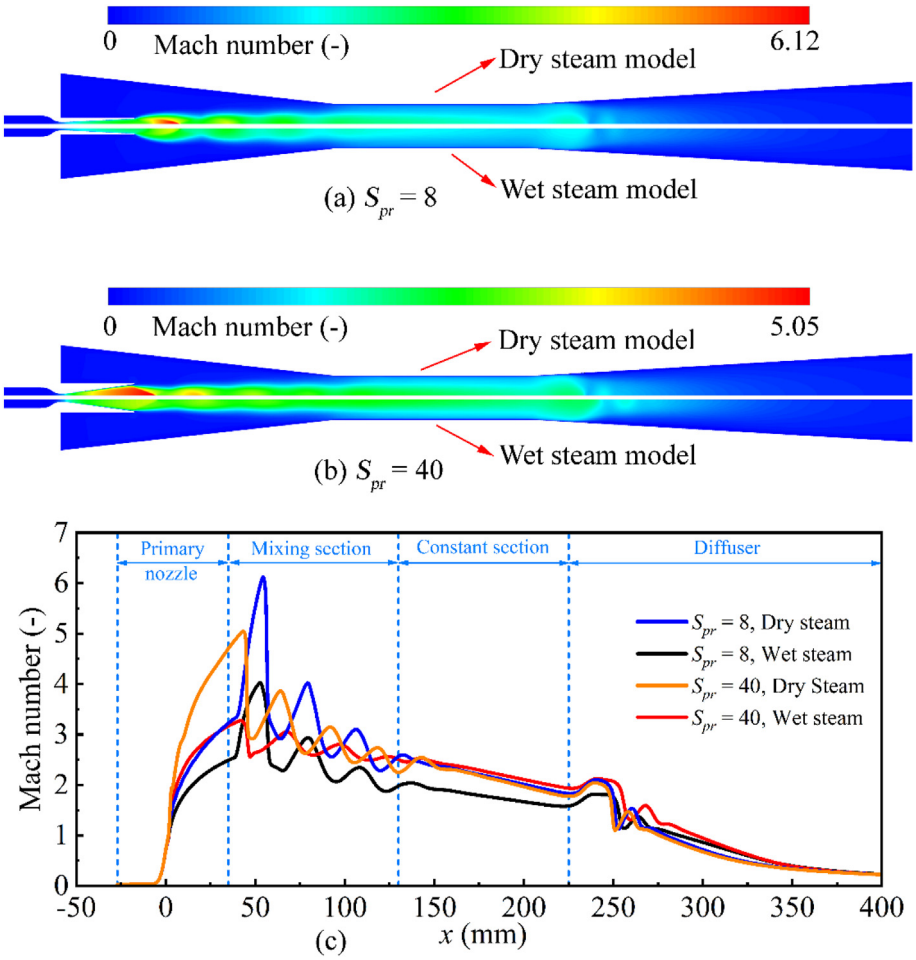

Fig. 18. Effect of wet steam and dry steam models on the Mach number in the steam ejector at the area ratios of the primary nozzle, S_{pr} = 8 and S_{pr} = 40.

shock wave than wet steam simulations in the diffuser.

Fig. 19 represents the entrainment ratio predicted by the two models in the steam ejector at different area ratios of the primary nozzle. It can be found that the over-prediction of the steam expansion results in higher entrainment performance for the area ratio of the primary nozzle of S_{pr} = 8–40. In general, the dry steam model both over-predicts the steam expansion and entrainment ratio in steam ejectors due to the neglect of the phase change behaviour. The wet steam model is suggested to evaluate the steam ejector performance considering the advantage of involving the heat and mass transfer in nonequilibrium condensation processes.

5. Conclusions

We test four different RANS turbulence models for the CFD modelling of steam ejectors, and our results show that the *k*-ω SST model produces the most accurate results when compared to experimental results. The wet steam model shows that the degree of subcooling can reach 50 K to generate a maximum liquid fraction of 0.26 in the steam ejector. However, the following compression process of the supersonic flow results in a steep decrease of the degree of subcooling to −60 K, which induce the evaporation of the condensed droplets. The condensation-evaporation processes may repeat alternatively in the mixing section depending on expansion-compression supersonic flows in the steam ejector.

When the area ratio of the primary nozzle increases from 8 to 26, the entrainment ratio decreases by 6.7% from 0.75 to 0.70 and the averaged liquid fraction increases by 45% from 0.0069 to 0.010 in the steam ejector. Increasing the area ratio from 26 to 40 leads to the transition of the flow structure from under-expanded flows to over-expanded flows in the mixing section. The droplet diameter is

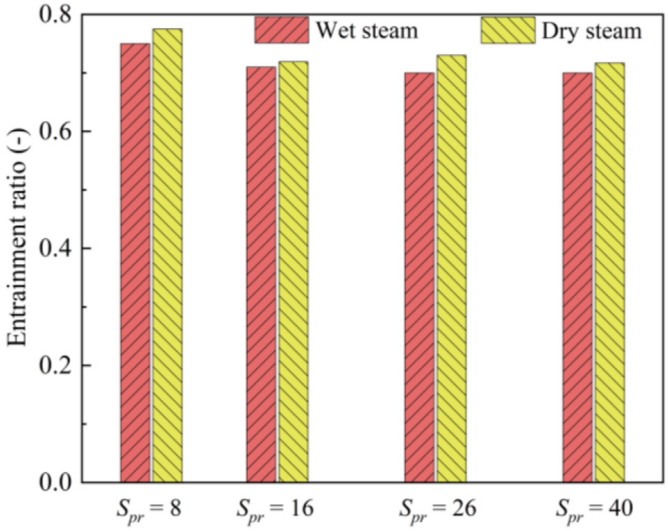

Fig. 19. Effect of wet steam and dry steam models on entrainment ratios in the steam ejector at different area ratios of the primary nozzle (S_{pr}).

about 7 nm in the constant section and the entrainment ratio can reach approximately 0.75 for the area ratio of the primary nozzle of 8, which achieves a satisfactory performance. The dry steam calculates a maximum Mach number of 6.12, while the wet steam model calculates the peak value of 4.02 for the area ratio of the primary nozzle of 8. This shows that the dry steam model overpredicts the steam expansion in the steam ejector owing to ignoring the phase change process.

The numerical simulation demonstrates that the wet steam model significantly influences the flow prediction in steam ejectors, which is not fully understood by assuming a dry steam flow. The interaction between the condensation process and the mixing process needs to be further investigated using a wet steam model.

Author statement

Yan Yang: Conceptualization, Methodology, Investigation, Writing – original draft preparation and revising, Nikolas Karvounis: Formal analysis, Writing - review and revising, Jens Honore Walther: Formal analysis, Writing - review and revising, Hongbing Ding: Methodology, Writing - review and revising, Chuang Wen: Conceptualization, Methodology, Writing - review and revising, Supervision

Declaration of competing interest

The authors declare that they have no known competing financial interests or personal relationships that could have appeared to influence the work reported in this paper.

Acknowledgements

This project has received funding from the European Union's Horizon 2020 research and innovation programme under the Marie Sklodowska-Curie grant agreement No 792876, the Independent Research Fund Denmark grant 8022-00143B, the Innovation Fund of Denmark and MAN Energy Solutions through the SULCOR project and the National Natural Science Foundation of China under Grant 51876143.

References

[1] Besagni G. Ejectors on the cutting edge: the past, the present and the perspective. Energy 2019;170:998–1003.
[2] Zhang G, Dykas S, Li P, Li H, Wang J. Accurate condensing steam flow modeling in the ejector of the solar-driven refrigeration system. Energy 2020;212:118690.
[3] Yang Y, Zhu X, Yan Y, Ding H, Wen C. Performance of supersonic steam ejectors considering the nonequilibrium condensation phenomenon for efficient energy utilisation. Appl Energy 2019;242:157–67.
[4] Tang Y, Liu Z, Li Y, Zhao F, Fan P, Chua KJ. Mixing process of two streams within a steam ejector from the perspectives of mass, momentum and energy transfer. Appl Therm Eng 2020:116358.
[5] Tashtoush B, Hasan A. A novel hybrid solar ejector cooling system with thermoelectric generators. Energy 2020:117318.
[6] Wen C, Rogie B, Kærn MR, Rothuizen E. A first study of the potential of integrating an ejector in hydrogen fuelling stations for fuelling high pressure hydrogen vehicles. Appl Energy 2020;260:113958.
[7] Tang Y, Liu Z, Li Y, Yang N, Wan Y, Chua KJ. A double-choking theory as an explanation of the evolution laws of ejector performance with various operational and geometrical parameters. Energy Convers Manag 2020;206:112499.
[8] Poirier M, Giguère D, Sapoundjiev H. Experimental parametric investigation of vapor ejector for refrigeration applications. Energy 2018;162:1287–300.
[9] Tang Y, Liu Z, Li Y, Shi C, Lv C. A combined pressure regulation technology with multi-optimization of the entrainment passage for performance improvement of the steam ejector in MED-TVC desalination system. Energy 2019;175:46–57.
[10] Ramesh AS, Sekhar SJ. Experimental and numerical investigations on the effect of suction chamber angle and nozzle exit position of a steam-jet ejector. Energy 2018;164:1097–113.
[11] Wang K, Wang L, Jia L, Cai W, Gao R. Optimization design of steam ejector primary nozzle for MED-TVC desalination system. Desalination 2019;471:114070.
[12] Ariafar K, Buttsworth D, Al-Doori G, Sharifi N. Mixing layer effects on the entrainment ratio in steam ejectors through ideal gas computational simulations. Energy 2016;95:380–92.
[13] Tang Y, Liu Z, Li Y, Huang Z, Chua KJ. Study on fundamental link between mixing efficiency and entrainment performance of a steam ejector. Energy 2021;215:119128.
[14] Suvarnakuta N, Pianthong K, Sriveerakul T, Seehanam W. Performance analysis of a two-stage ejector in an ejector refrigeration system using computational fluid dynamics. Eng Appl Comput Fluid Mechanics 2020;14:669–82.
[15] Liu J, Wang L, Jia L, Wang X. The influence of the area ratio on ejector efficiencies in the MED-TVC desalination system. Desalination 2017;413:168–75.
[16] Liu J, Wang L, Jia L, Xue H. Thermodynamic analysis of the steam ejector for desalination applications. Appl Therm Eng 2019;159:113883.
[17] Tang Y, Liu Z, Li Y, Wu H, Zhang X, Yang N. Visualization experimental study of the condensing flow regime in the transonic mixing process of desalination-oriented steam ejector. Energy Convers Manag 2019;197:111849.
[18] Ariafar K, Buttsworth D, Sharifi N, Malpress R. Ejector primary nozzle steam condensation: area ratio effects and mixing layer development. Appl Therm Eng 2014;71:519–27.
[19] Wang C, Wang L, Zou T, Zhang H. Influences of area ratio and surface roughness on homogeneous condensation in ejector primary nozzle. Energy Convers Manag 2017;149:168–74.
[20] Marynowski T, Desevaux P, Mercadier Y. Experimental and numerical visualizations of condensation process in a supersonic ejector. J Visual 2009;12:251–8.
[21] Sharifi N, Boroomand M, Sharifi M. Numerical assessment of steam nucleation on thermodynamic performance of steam ejectors. Appl Therm Eng 2013;52:449–59.
[22] Zhang G, Zhang X, Wang D, Jin Z, Qin X. Performance evaluation and operation optimization of the steam ejector based on modified model. Appl Therm Eng 2019;163:114388.
[23] Wen C, Ding H, Yang Y. Performance of steam ejector with nonequilibrium condensation for multi-effect distillation with thermal vapour compression (MED-TVC) seawater desalination system. Desalination 2020;489:114531.
[24] Mazzelli F, Giacomelli F, Milazzo A. CFD modeling of condensing steam ejectors: comparison with an experimental test-case. Int J Therm Sci 2018;127:7–18.
[25] Zhang G, Dykas S, Yang S, Zhang X, Li H, Wang J. Optimization of the primary nozzle based on a modified condensation model in a steam ejector. Appl Therm Eng 2020;171:115090.
[26] Faghih Aliabadi MA, Bahiraei M. Effect of water nano-droplet injection on steam ejector performance based on non-equilibrium spontaneous condensation: a droplet number study. Appl Therm Eng 2020:116236.
[27] Yang X, Long X, Yao X. Numerical investigation on the mixing process in a steam ejector with different nozzle structures. Int J Therm Sci 2012;56:95–106.
[28] Sharifi N, Sharifi M. Reducing energy consumption of a steam ejector through experimental optimization of the nozzle geometry. Energy 2014;66:860–7.
[29] Fu W, Li Y, Liu Z, Wu H, Wu T. Numerical study for the influences of primary nozzle on steam ejector performance. Appl Therm Eng 2016;106:1148–56.
[30] Wu Y, Zhao H, Zhang C, Wang L, Han J. Optimization analysis of structure parameters of steam ejector based on CFD and orthogonal test. Energy 2018;151:79–93.
[31] Strušnik D, Golob M, Avsec J. Effect of non-condensable gas on heat transfer in steam turbine condenser and modelling of ejector pump system by controlling the gas extraction rate through extraction tubes. Energy Convers Manag 2016;126:228–46.
[32] Strušnik D, Marčič M, Golob M, Hribernik A, Živić M, Avsec J. Energy efficiency analysis of steam ejector and electric vacuum pump for a turbine condenser air extraction system based on supervised machine learning modelling. Appl Energy 2016;173:386–405.
[33] Wen C, Gong L, Ding H, Yang Y. Steam ejector performance considering phase transition for multi-effect distillation with thermal vapour compression (MED-TVC) desalination system. Appl Energy 2020;279:115831.
[34] Atmaca M, Ezgi C. Three-dimensional CFD modeling of a steam ejector. Energy Sources A: Recovery Util Environ Effects 2019:1–12.
[35] Pianthong K, Seehanam W, Behnia M, Sriveerakul T, Aphornratana S. Investigation and improvement of ejector refrigeration system using computational fluid dynamics technique. Energy Convers Manag 2007;48:2556–64.
[36] Sharifi N. Axisymmetric and three dimensional flow modeling within thermal vapor compressors. Heat Mass Tran 2013;49:1489–501.
[37] Dykas S, Majkut M, Smołka K, Strozik M. Comprehensive investigations into thermal and flow phenomena occurring in the atmospheric air two-phase flow through nozzles. Int J Heat Mass Tran 2017;114:1072–85.
[38] Dykas S, Wróblewski W. Numerical modelling of steam condensing flow in low and high-pressure nozzles. Int J Heat Mass Tran 2012;55:6191–9.
[39] Wen C, Karvounis N, Walther JH, Ding H, Yang Y. Non-equilibrium condensation of water vapour in supersonic flows with shock waves. Int J Heat Mass Tran 2020;149:119109.
[40] Wen C, Karvounis N, Walther JH, Yan Y, Feng Y, Yang Y. An efficient approach to separate CO2 using supersonic flows for carbon capture and storage. Appl Energy 2019;238:311–9.
[41] Wen C, Ding H, Yang Y. Optimisation study of a supersonic separator

considering nonequilibrium condensation behaviour. Energy Convers Manag 2020;222:113210.
[42] Kantrowitz A. Nucleation in very rapid vapor expansions. J Chem Phys 1951;19:1097–100.
[43] Young J. The spontaneous condensation of steam in supersonic nozzle. Physio Chem Hydrodynamics 1982;3:57–82.
[44] Starzmann J, Hughes FR, Schuster S, White AJ, Halama J, Hric V, et al. Results of the international wet steam modeling project. Proc IME J Power Energy 2018;232:550–70.
[45] ANSYS Fluent theory guide. USA: ANSYS Inc; 2017.
[46] Wen C, Ding H, Yang Y. Numerical simulation of nanodroplet generation of water vapour in high-pressure supersonic flows for the potential of clean natural gas dehydration. Energy Convers Manag 2021;231:113853.
[47] Majidi D, Farhadi F. Supersonic separator's dehumidification performance with specific structure: experimental and numerical investigation. Appl Therm Eng 2020;179:115551.
[48] Gyarmathy G. Nucleation of steam in high-pressure nozzle experiments. Proc IME J Power Energy 2005;219:511–21.
[49] Am Binnie M, Green J, Be D. An electrical detector of condensation in high-velocity steam. Proc Roy Soc Lond A 1942;181:134–54.
[50] Hunter CA. Experimental investigation of separated nozzle flows. J Propul Power 2004;20:527–32.
[51] Sriveerakul T, Aphornratana S, Chunnanond K. Performance prediction of steam ejector using computational fluid dynamics: Part 1. Validation of the CFD results. Int J Therm Sci 2007;46:812–22.